Towards 3D lidar point cloud registration improvement using optimal neighborhood knowledge

Adrien Gressin, Clément Mallet, Jérôme Demantké, Nicolas David

Towards 3D lidar point cloud registration improvement using optimal neighborhood knowledge.

Adrien Gressin, Clément Mallet, Jérôme Demantké, Nicolas David
Université Paris-Est – IGN/SR, MATIS, 73 avenue de Paris, 94160 Saint-Mandé, France

Abstract

Automatic 3D point cloud registration is a main issue in computer vision and remote sensing. One of the most commonly adopted solution is the well-known Iterative Closest Point (ICP) algorithm. This standard approach performs a fine registration of two overlapping point clouds by iteratively estimating the transformation parameters, assuming good a priori alignment is provided. A large body of literature has proposed many variations in order to improve each step of the process (namely selecting, matching, rejecting, weighting and minimizing). The aim of this paper is to demonstrate how the knowledge of the shape that best fits the local geometry of each 3D point neighborhood can improve the speed and the accuracy of each of these steps. We first present the geometrical features that are the basis of this work. These low-level attributes indeed describe the neighborhood shape around each 3D point. They allow to retrieve the optimal size for analyzing the neighborhoods at various scales as well as the privileged local dimension (linear, planar, or volumetric). Several variations of each step of the ICP process are then proposed and analyzed by introducing these features. Such variants are compared on real datasets, as well with the original algorithm in order to retrieve the most efficient algorithm for the whole process. The method is therefore successfully applied to various 3D lidar point clouds from airborne, terrestrial, and mobile mapping systems. Improvements are noticed for two of the five ICP steps, while concluding our features may not be relevant for very dissimilar object samplings.

Keywords: Point cloud, registration, ICP, eigenvalues, dimensionality,

neighborhood, change detection

1. Introduction

1.1. Why registering 3D topographic point clouds ?

Lidar systems provide 3D point clouds with increasing accuracy and reliability. When the same area of interest is acquired twice, or more, over time or space, depending of the application, the registration problem arises. For airborne and mobile platforms, the use of an hybrid IMU (Inertial Measurement Unit)/GPS georeferencing system introduce 3D shifts between 3D point clouds. For airborne surveys, this mainly comes from drifts of the inertial measurement unit. One has to solve the so-called strip registration issue: planimetric and altimetric discrepancies exist between two overlapping strips at a level superior to the sensor noise (up to 2 m in altimetry). When dealing with mobile mapping systems in urban corridors, the problem is increased by GPS signal gaps, resulting in significant shifts in platform trajectory estimation, as well as by the presence of moving objects such as cars and pedestrians. For static terrestrial devices, registration is required when several points of view of the same object are acquired, facing the issue of putting them in correspondence with few overlapping areas and varying point densities (Lichti and Skaloud, 2010). Consequently, alignment of several point clouds remains a prerequisite for subsequent analysis and processing steps.

1.2. Existing solutions

In the literature, a plethora of papers have addressed the problem of 3D data registration, alternatively in terms of point cloud alignment or range image matching. Both rigid and non-rigid methods exists.

One can coarsely divide the 3D point cloud registration algorithms in three main families. Firstly, the alignment using feature-based methods is achieved through the correspondence of feature primitives or keypoints, that, in addition, may have interesting properties with respects to the issue of interest (*e.g.*,

invariant to rigid-motion). Such methods therefore heavily rely on the primitive extraction step, but the subsequent matching step allows to avoid several standard issues such as noise, outlier detection and large data volume management. Features can be keypoints (SIFT, spin images) (Huber and Hebert, 2003b; Stamos and Leordeanu, 2003; Barnea and Filin, 2008; Weinmann et al., 2011), corners (Thirion, 1996), segment or curves (Stein and Medioni, 1992), local planes (Dold and Brenner, 2006), specific patterns (spheres, cylinders) or higher-level shape descriptors (Frome et al., 2004). The exhaustive search of corresponding feature pairs can be leveraged using pruning or selection techniques (such as RANSAC) or efficient hierarchical optimization techniques.
Secondly, in surface-based approaches, 3D datasets are represented by a surface model. Usually, the model used for registration is the mesh model. Then, the registration is performed directly on mesh models rather than on the 3D point cloud. The introduction of surfaces allows to take into account holes, potential deformation between them and the introduction of well-established techniques such as thin-plate splines (Szeliski and Lavallée, 1996; Allen et al., 2003; Chui et al., 2004; Mitra et al., 2004).
Finally, one can find non-focused point-based methods, requiring neither feature extraction nor pre-modeling step. They may work on the full set of points or on specific subsets. Their aim is (1) to find correspondences between the two point sets and (2) to estimate the transformation. These methods can classified according to:

- The performance of these two steps, simultaneously or sequentially;
- The type of the underlying optimization method used, which can global or local, some authors even trying to mix both levels of information (Breitenreicher and Schnörr, 2011; Papazov and Burschka, 2011).

Simultaneous methods are known to be very robust since the errors are distributed among all the points of the sets to limit distortion with preserving the geometry (Huber and Hebert, 2003a; Myronenko and Song, 2010). Although, their major deficiencies are the actual computation time, and the potential loss

of small details owing to error accumulation. Sequential methods may produce imprecise results since errors can be more easily propagated, unless one can guarantee initial correct alignment (Chen and Medioni, 1992).

Global, deterministic or stochastic, optimizations using for instance branch-and-bound methods, simulated annealing, genetic algorithms, or evolutionary methods also exhibit significant computing times (especially deterministic ones, but with guaranteed convergence), and are generally regarded as providing coarse registration (Silva et al., 2005). They therefore can be coupled with local methods, even if some authors manage to reach global minima without any initialization (Li and Hartley, 2007). The landmark contribution in local family is the Iterative Closest Point (ICP) algorithm. We have selected it for our study since this is one of the most widespread method to compute registration of two point clouds. Other methods based on the Least-squares procedure (Gruen and Akca, 2005; Grant et al., 2012), the Random Sample Consensus algorithm (Chen et al., 1999), kernel correlation (Tsin and Kanade, 2004) or the Normal Distribution Transform (Ripperda and Brenner, 2005) exist, and can have more interesting convergence properties than the ICP. It iteratively minimize the mean square error between points in point set and the closest points in the other one. The simplicity of this method, introduced by Chen and Medioni (1992) and Besl and McKay (1992), is the reason for its extensive use for a large variety of datasets and contexts. Nevertheless, due to sensibility of the iterative method to noise and poor iteration, many variants have been developed to improve the five consecutive steps (*selecting*, *matching*, *rejecting* and *weighting* compose the correspondence finding part whereas the transformation estimate consists in *minimizing* a given function), with varying degrees of success and more or less focused on specific issues (mainly convergence speed versus accuracy) (Lu and Milos, 1997; Rusinkiewicz and Levoy, 2001; Gelfand et al., 2003; Segal et al., 2009; Bae, 2010). The ICP is only valid for pair-wise registration, and other methods are required for the simultaneous registration of multiple point clouds (Craciun et al., 2010). According to Rodrigues et al. (2002), no optimal solutions exists. For the time being, the ICP method is still the state-of-the-art

algorithm (Salvi et al., 2007).

1.3. Feature introduction in ICP

Since ICP is an iterative descent algorithm, it requires a good initial estimation so as to converge to the global minimum. Besides, the ICP matching step is the most time-consuming part of the registration phase, thus improving the rate of convergence is crucial to make registration faster. To reduce the matching time, effective features of interest should be found. Such attributes may also be relevant to cope with erroneous associations between nearest points. This can frequently happen in case of surfaces or objects acquired with different point densities or different points of view in the two datasets (Salvi et al., 2007). Consequently, two main solutions have been proposed in literature: working at object level (Douillard et al., 2012) or computing, for each point, local features providing neighborhood information. Thus, several interesting local descriptors, based on the geometrical point cloud analysis, have been elaborated, and successfully used on ICP variants. For instance, Bae and Lichti (2008) have recently focused on the analysis of the geometrical curvature and the position uncertainty of laser scanner measurement. The introduction of features of interest seems indeed very effective, since it allows to focus the registration process on the most reliable regions. The "reliability" may be evaluated according to planar criteria or with scale-space analysis (Sharp et al., 2002; Ho et al., 2009). For more complex environments with specific patterns other primitives may be introduced, for example shapes like planar patches, spheres, cylinders and tori in industrial areas (Rabbani et al., 2007).

Recently, several authors have focused on multi-scale local 3D point analysis for several purposes: dimension filtering for suitable operator definition (Unnikrishnan and Hebert, 2008; Digne and Morel, 2012), line extraction (Pauly et al., 2003), normal vector estimation (Unnikrishnan et al., 2010) and propagation (Digne et al., 2011) or 3D model compactness analysis (Novatnack and Nishino, 2007). In (Demantké et al., 2011) and (Brodu and Lague, 2012), the multi-scale

analysis of 3D lidar points, based solely on the geometrical information allows to retrieve for each point the optimal neighborhood size and the prominent behaviour of the vicinity (linear, planar, or volumetric).

1.4. Motivation

The aim of this paper is to propose a general and automatic method for 3D point cloud alignment, applicable on the three kinds of topographic lidar datasets mentioned in Section 4. We focus on pair-wise registration of datasets that do not exhibit large changes (especially in rotation), the coarse 3D registration issue being beyond the scope of this article. Furthermore, finding the correspondence between a lidar dataset and an existing 3D model (Bosché, 2012) or a photogrammetric point cloud (Armenakis et al., 2012) are not investigated here. We assume the existence of a good a priori alignment before the two point sets of interest. If not, when scan orientations are unknown (*e.g.*, terrestrial surveys), methods specific to the areas of interest are required (Makadia et al., 2006; Barnea and Filin, 2008; Theiler and Schindler, 2012).
Specifically, our goal is to assess how the introduction of the multi-scale features of Demantké et al. (2011), simply computed on 3D points, may improve a standard fine-registration algorithm, namely the Iterative Closest Point method.
This paper extends the work we presented in (Gressin et al., 2012) by detailing and improving the geometrical features selection, and by presenting new results. The geometrical features of interest are first introduced (Section 2). Then, the five steps of the ICP algorithm are described in Section 3. For each step, the introduction of the proposed features is discussed. After a short presentation of the datasets in Section 4, the different variants of the ICP algorithm are evaluated and compared in Section 5. This allows to propose an optimized combination of ICP variants. Finally, conclusions are drawn in Section 6.

2. Finding features of interest

Our goal is to introduce the geometrical features that have been proposed in (Demantké et al., 2011) in the ICP procedure. The method aims to find, for each

3D point, the optimal neighborhood size. The primary goal was to find the most suitable local point set facing the interdependence problem: geometrical features depend on the choice of the neighborhood, whereas a good neighborhood choice should rely on the local geometry, and thus on geometrical features.
This is a two-step approach. In a first time, dimensionality features (1D, 2D, 3D) are proposed for a given neighborhood size of spherical shape. Then, these features are computed for growing sizes, and the neighborhood radius is adjusted in order to minimize an entropy function. This provides the most salient scale of analysis and the associated dimension. The proposed method exhibits several advantages that are likely to be relevant for our purpose:

- The simple knowledge of the three geographical coordinates is sufficient (no *intensity* information) : the features of interest are based on the covariance matrix populated with the second order moment of the {x,y,z} triplets.
- The method has been successfully applied to the three main kinds of lidar point clouds (airborne, terrestrial static, mobile mapping system);
- It does not rely on properties of specific objects or on structured datasets;
- In addition to the optimal search radius, the local point set behaviour (linear, planar, or scatter) is retrieved.

2.1. Dimensionality features

For each point P, points closer than distance r (radius) belong to a spherical neighborhood $\mathcal{V}^r$ centered on P. A Principal Component Analysis is performed on such point set to obtain three eigenvalues $(\lambda_1, \lambda_2, \lambda_3)$, such as $\lambda_1 \geq \lambda_2 \geq \lambda_3 \geq 0$, and three eigenvectors $(\overrightarrow{v_1}, \overrightarrow{v_2}, \overrightarrow{v_3})$. One can note that $\overrightarrow{v_3}$ provides a robust value of the normal of the 3D point, noted hereafter $\overrightarrow{n}$. The standard deviation along an eigenvector i is denoted by:

$$\forall\, i \in [1,3],\ \sigma_i = \sqrt{\lambda_i}. \tag{1}$$

The shape of the point distribution within $\mathcal{V}^r$ is then represented by an oriented ellipsoid. Three geometrical features are introduced in order to describe the linear ($a_{1\mathrm{D}}$), planar ($a_{2\mathrm{D}}$) or scatter ($a_{3\mathrm{D}}$) behaviors within $\mathcal{V}^r$:

$$a_{1\mathrm{D}} = \frac{\sigma_1 - \sigma_2}{\sigma_1}, \quad a_{2\mathrm{D}} = \frac{\sigma_2 - \sigma_3}{\sigma_1}, \quad a_{3\mathrm{D}} = \frac{\sigma_3}{\sigma_1}. \tag{2}$$

These three features are normalized so that $a_{1D} + a_{2D} + a_{3D} = 1$. This allows to consider them as the probabilities of each point to be labeled as linear (1D), planar (2D) or volumetric (3D). These low-level primitives are considered to be sufficient to describe the main behaviours within a point cloud (see Figure 1). Since the method is designed to be independent to any information about the acquisition process (objects, point density, scan pattern, etc.), additional geometrical description would introduce noise in the process, and, thus, make the process less general. For the specific case of airborne laser scanning, the reader should refer to (Jutzi and Gross, 2009), where a more complete analysis is performed on which kinds of geometrical behaviours can be detected and labeled. The dimensionality label l^* (1D, 2D, or 3D) of $\mathcal{V}^r$ is defined by:

$$l^*(\mathcal{V}^r) = \underset{l \in [1,3]}{\arg\max} [a_{\mathrm{l}\mathrm{D}}]. \tag{3}$$

If $\sigma_1 \gg \sigma_2, \sigma_3$, then $a_{1\mathrm{D}}$ is greater than the two other features, and the dimensionality label $l^*(\mathcal{V}^r)$ results to 1. This corresponds to edges between planar surfaces, catenary curves, poles, traffic lights, thin tree trunks etc. Conversely, in case of planar surface or slightly curved areas, $\sigma_1, \sigma_2 \gg \sigma_3$, and $a_{2\mathrm{D}}$ will prevail. Finally, $\sigma_1 \simeq \sigma_2 \simeq \sigma_3$ implies $l^*(\mathcal{V}^r) = 3$, corresponding to spatially scattered objects such as vegetation.

2.2. Optimal neighborhood radius

The dimensionality features are computed for increasing radii values between a lower bound $r_{\min}$ to an upper bound $r_{\max}$, using a square factor. Demantké et al. (2011) describe how these bounds can be automatically retrieved, and how the $[r_{\min}, r_{\max}]$ space can be efficiently sampled.

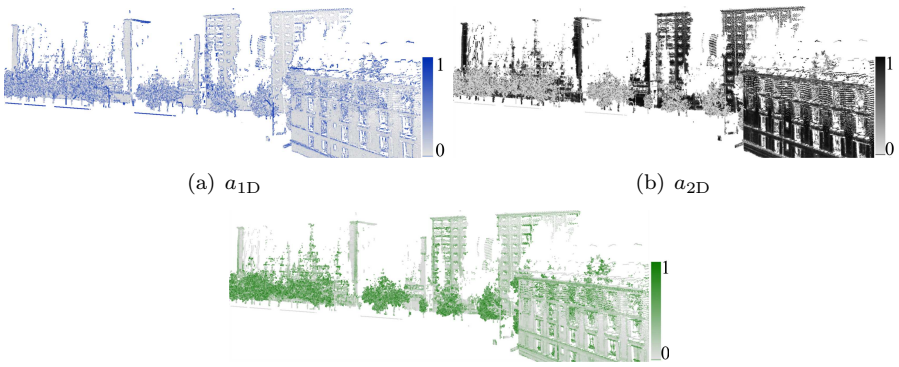

(a) a_{1D} (b) a_{2D}

(c) a_{3D}

Figure 1: Illustration of the three low-level descriptors over building facades acquired with a Mobile Mapping System.

For each radius r, and for each lidar point P, a measure of unpredictability is given by the Shannon entropy of the discrete probability distribution (a_{1D}, a_{2D}, a_{3D}):

$$E_f(\mathcal{V}_p^r) = -a_{1D}\ln(a_{1D}) - a_{2D}\ln(a_{2D}) - a_{3D}\ln(a_{3D}). \tag{4}$$

Then, the optimal neighborhood radius is obtained as the minimum of the entropy function E_f (cf. Figure 2):

$$r_P^* = \underset{r\in[r_{\min},\, r_{\max}]}{\arg\min}\; E_f(\mathcal{V}_P^r). \tag{5}$$

The optimal neighborhood $\mathcal{V}^*$, associated to r^* is finally used to compute a dimensionality label $l^*(\mathcal{V}_P^{r^*})$, noted l^* in the following sections.

2.3. Features of interest

Various features have been computed in the previous section, and several others can be derived from them. One main feature of interest is the omnivariance $O = \prod_{i\in[1,3]} \sigma_i$ (Gross and Thoennessen, 2006), thus proportional to the ellipsoid volume. It allows to characterize the shape of the neighborhood, and, in particular, to enhance whether one or two eigenvalues are prominent.

Each 3D point of the cloud can then be described by the following feature set:

$$\{\lambda_1, \lambda_2, \lambda_3, \overrightarrow{v_1}, \overrightarrow{v_2}, \overrightarrow{v_3}, a_{1\mathrm{D}}, a_{2\mathrm{D}}, a_{3\mathrm{D}}, l^*, r^*, E_f^*, O\}, \tag{6}$$

with $E_f^* = E_f(\mathcal{V}_p^{r^*})$ and $\overrightarrow{v_3} = \overrightarrow{n}$.

One can note that $\overrightarrow{n}$ and O have been computed from the optimal neighborhood, and thus also benefit from the described method. $\overrightarrow{n}$ provides a robust approximation of the local surface normal. O allows a global description of the shape of the neighborhood. As we consider $\overrightarrow{n}$ being sufficient for representing the surface orientation, $\overrightarrow{v_1}$ and $\overrightarrow{v_2}$ are discarded for the subsequent relevance analysis. As the most suitable features for registration are not known beforehand, the other attributes are conserved so as to be integrated in the different ICP steps. Their specific contribution will be discussed at each of the analysed steps.

Figure 2 gives an illustration of several features for a building facade acquired with a Mobile Mapping System. One can see than the optimal radius, and thus the omnivariance increase for lower point densities, and that most of the facade is correctly described as a planar surface.

3. Optimizing the Iterative Closest Point algorithm

3.1. ICP steps

The purpose of ICP algorithm is to perform the registration of two coarsely aligned point clouds (a *mobile* point cloud registered on a fixed *reference* point cloud). It iteratively minimizes the distances of all points in the *reference* scan to the nearest point or plane in the *mobile* one. It is based on a squared-error and converges to a local minimum. More details can be found for instance in (Bae, 2010). The algorithm is composed of five steps detailed in the next section. First, a reduced number of points is selected to find suitable candidates for registration. Then, matching points are found between the two points clouds, and each corresponding pair is weighted. Some of these corresponding pairs may

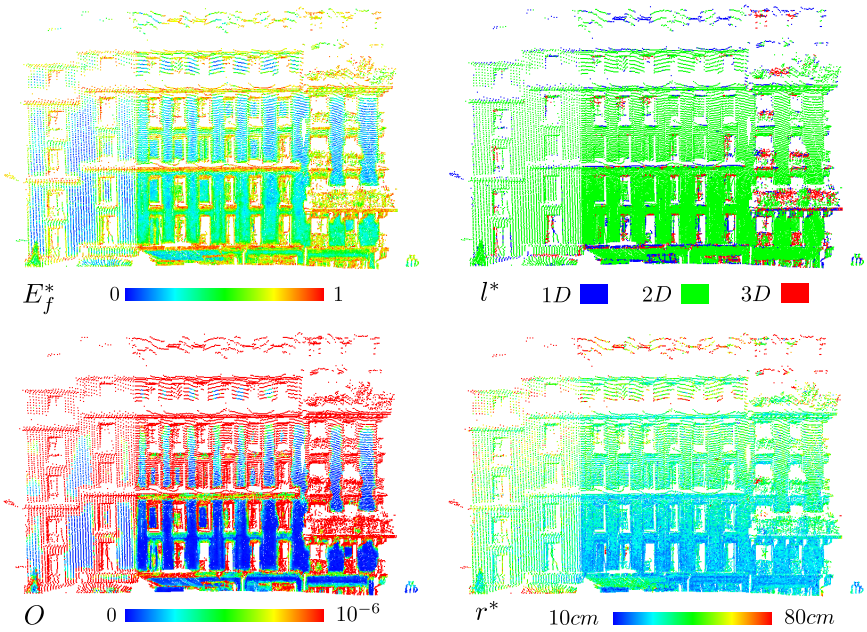

Figure 2: Several dimensionality features introduced in the ICP procedure.

be rejected. rejecting. Furthermore, an error metric is traditionally designed with respect to the context and the area of interest, and finally minimized, providing transformation parameters (translation and rotation). For each step, various variants and extensions exist so as to increase convergence, robustness, and computational efficiency (Bergevin et al., 1996; Rusinkiewicz and Levoy, 2001).

Selection aims to sample the two initial point clouds (mobile and reference point clouds) in order to reduce computation time caused by large data sets. Efforts on efficient selection will be performed here.

Matching deals with the search for (robust) corresponding point pairs. The simplest and the most widely adapted one is to find the closest point in the reference point cloud. Since this solution may be corrupted by noise or is sensitive to surface discretization, other methods use surfaces/meshes to compute

point-to-surface matching. Then, a compatibility metric can be designed to refine the matching, for example using color (Godin et al., 1994), normals (Pulli, 1999), high-order derivatives or other features mentioned in Section 1.3. Since, no underlying surface can be considered in our datasets, we have adopted the point-to-point strategy without any modification. We consider that the features derived in Section 2 allow an analysis on a larger, but still local, spatial support. Furthermore, we do not directly do the matching in a higher-dimensional space: the standard Euclidean distance is considered.

Weighting / Rejecting consists in adding some contextual knowledge for each corresponding pair of interest. Firstly, each of them can be weighted with respect to the neighborhood or the whole point cloud. The relevance of our feature set will be assessed. Secondly, the worst pairs may be rejected using, most of the times, statistics on the whole point cloud. Improvements will also be proposed here.

Minimizing. Given a set of matching points $\mathcal{C} = \{(P_i^{\text{mob}}, P_i^{\text{ref}})\}_i$ of two sets (*mobile* and *reference*), weighted with w_i, the purpose of the last step of the ICP algorithm is to find the transformation $\mathcal{T}$ minimizing the sum of the squared distances between each couple of points. The two most frequently adapted distances in the literature are the point-to-point distance, and the point-to-plane distance using the normal of each point. Since the local normal vector $\overrightarrow{n_i}$ is assumed to be (more) reliable thanks to the adopted multi-scale analysis, the second option is adopted. The optimal transformation $\mathcal{T}^*$ is computed as follows:

$$\mathcal{T}^* = \underset{\mathcal{T}}{\operatorname{argmin}} \sum_{i=1}^{\operatorname{card}(\mathcal{C})} w_i((\mathcal{T} * P_i^{\text{mob}} - P_i^{\text{ref}}) \cdot \overrightarrow{n_i})^2. \tag{7}$$

$\mathcal{T}^*$ corresponds in practice to a rotation matrix and a translation vector (Besl and McKay, 1992).

In the following sections, the variations of ICP steps with the inclusion of our geometrical features are described.

3.2. Selection step

A naive strategy is to randomly subsample the point cloud so that the general distribution of the points is preserved (Turk and Levoy, 1994). As a multi-scale analysis, different samples can also be performed at each iteration (Masuda et al., 1996). Another possibility is to select points with high intensity gradient if color or intensity is available (Godin et al., 1994). Rusinkiewicz and Levoy (2001) prefer selecting points so as to preserve a distribution of normals as large as possible.

As alternatives, two solutions based on E_f^* and l^* features are proposed. Such attributes allow to focus the selection step on the most reliable areas for accurate registration. An area is considered as "unreliable" if it corresponds to (1) the boundary between several objects or surfaces, or to (2) a geometrically complex object. In such cases, since the acquisition processes of the two point clouds may be distinct, the local geometries are likely to be dissimilar.

- **High-entropy selection**: As described in Section 2.2, the larger E_f^*, the more prominent a single dimension. This means that the local geometry is simple enough to take a strong decision, thus pointing out salient regions of the 3D point cloud (Figure 2).

- **Dimensionality-based selection**: Three variants are tested, corresponding to the three possible values of l^*.

  - $l^* = 1$ corresponds to linear behaviour *i.e.*, borders between surfaces or thin objects (Demantké et al., 2011). They are strong cues for registration if their sampling in both datasets is sufficient.

  - $l^* = 2$ will keep planar surfaces that are likely to be the most stable areas of interest for matching.

  - Scattered objects correspond to $l^* = 3$. Since few objects are labeled as volumetric in practice, few points will be selected.

3.3. Weighting step

After searching corresponding pairs, each of them is weighted. Several weighting functions of two points (P_1, P_2) exist in the literature (Godin et al., 1994). Basically, a constant weighting function $w_C(P_1, P_2) = w_0$ (w_0 being arbitrarily set) is chosen. Another strategy consists in adding a weighting function d: $w_D(P_1, P_2) = 1 - \frac{d(P_1,P_2)}{d_{\max}}$, where $d_{\max}$ is the maximum value of this function for the set of pairs.

The Euclidian norm $d(.) = d_2(.) = \|.\|$ is often used. Since specific geometrical features have been introduced, an omnivariance compatibility metric $d_O(p_1, p_2)$ is first proposed. It is based on the difference of the ellipsoid volumes O. Thus, a weighting function $w_O(P_1, P_2)$ is designed as follows:

$$w_O(P_1, P_2) = 1 - \frac{d_O(P_1, P_2)}{d_{\max}}, \quad \text{with } d_O(P_1, P_2) = |O_{P_1} - O_{P_2}|. \tag{8}$$

Similarly, three other weighting functions are introduced, based on three different distances and features (namely the eigenvalues λ, the geometrical features a, and the optimal radii r):

- $w_\lambda(P_1, P_2) = 1 - \frac{d_\lambda(P_1,P_2)}{d_{\max}}$, with $d_\lambda(P_1, P_2)^2 = \sum_{i=1}^{3}(\lambda_i^1 - \lambda_i^2)^2$;
- $w_a(P_1, P_2) = 1 - \frac{d_a(P_1,P_2)}{d_{\max}}$, with $d_a(P_1, P_2)^2 = \sum_{i=1}^{3}(a_{iD}^1 - a_{iD}^2)^2$;
- $w_r(P_1, P_2) = 1 - \frac{d_r(P_1,P_2)}{d_{\max}}$, with $d_r(P_1, P_2) = |(r^1 - r^2)|$.

Finally, normal compatibility can be inserted to define another weighting function: $w_N(P_1, P_2) = \overrightarrow{n_1}.\overrightarrow{n_2}$. Since normal computation has been improved using the method of (Demantké et al., 2011), this solution is also tested.

3.4. Rejecting step

The literature generally proposes to reject the worst corresponding pairs, based on various distance criteria:

- Distance threshold such as 2.5 times the standard deviation of distances of pairs (Masuda et al., 1996);

- Rank filter: n% with the greatest distance (Pulli, 1999).

The rejection distance being not necessarily the same as for the matching step, different distances are adopted in order to discard the worst corresponding pairs:

- n% with the greatest distance, using d_O;
- n% with the greatest distance, using d_a;
- n% with the greatest distance, using d_r;
- n% with the greatest distance, using d_{dim}.

The distances d_O, d_a, and d_r have been introduced in Section 3.3. In addition, we have for a pair of points (P_1, P_2): $d_{\text{dim}}(P_1, P_2) = d_2(P_1, P_2)$ if $(l_1^* = l_2^*)$ and $d_{\text{dim}}(P_1, P_2) = \infty$ otherwise.

4. Datasets

Three kinds of lidar datasets are exploited in order to assess the relevance and performance of each proposed variant of the algorithm. These datasets have various point densities, point distribution, and points of view since they have been acquired with different lidar systems: airborne (ALS), terrestrial static (TLS), and mobile mapping systems (MMS).

4.1. ALS

The dataset has been acquired over a dense urban area (city center with low-elevated buildings, cf. Figure 3) at two different dates, and with distinct airborne lidar scanners, resulting in two different ground patterns. The first acquisition (ALS_{03}) was completed in 2003 (point density of 7.5 pts/m^2, $400,000$ pts), with a Toposys fiber scanner (Lohr and Eibert, 1995). The spatial sampling is therefore very inhomogeneous (1.5m between two fibers, and 0.15m between two measurements of the same fiber). The second acquisition (*ALS 08*) occurred in 2008 (point density of 2 pts/m^2, $90,000$ pts, oscillating mirror) with an Optech

3100 EA device. Registering these two epochs is crucial for change detection purposes (Figure 3).

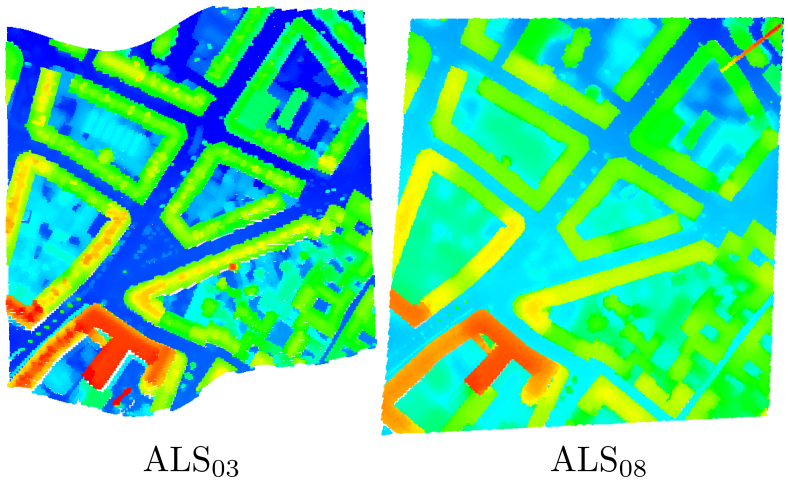

Figure 3: Two ALS datasets. ALS_{03} and ALS_{08} correspond to point clouds acquired in 2003 and 2008, respectively.

4.2. TLS

The *TLS* concerns an indoor environment (point density of 0.3 pt/cm^2, 20,000 pts). Two points of view of the same area (office desk covered with various objects) were consecutively acquired with the same Trimble system (Figure 4), and slightly different points of view. One can see that an object (a house plant) has also been removed.

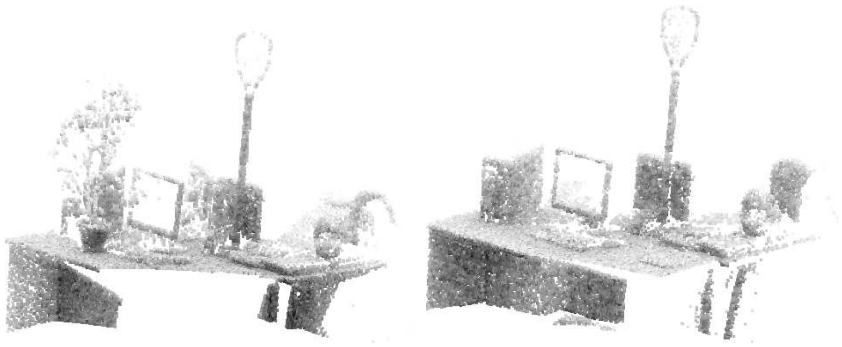

Figure 4: TLS dataset, with two points of view, colored using ambient occlusion.

4.3. MMS

This dataset covers one building facade in an urban area in France (Figure 5). The mobile mapping system acquired two times the same area the same day but with a time shift of one hour. A RIEGL LMS-Q120i lidar has been used for that purpose, and oriented towards the roof top (pavement and road surfaces omitted).

The challenges are that: (1) not exactly the same parts of the buildings are sampled, and (2) a 3D shift between both point clouds naturally exists, due to georeferencing process. The point cloud density is very variable, even inside the same point cloud, depending on the angle of incidence of the variable distance between objects and the MMS. However, the typical density on the facades of the buildings is near 100 pts/m^2 (around $200,000$ pts per point cloud).

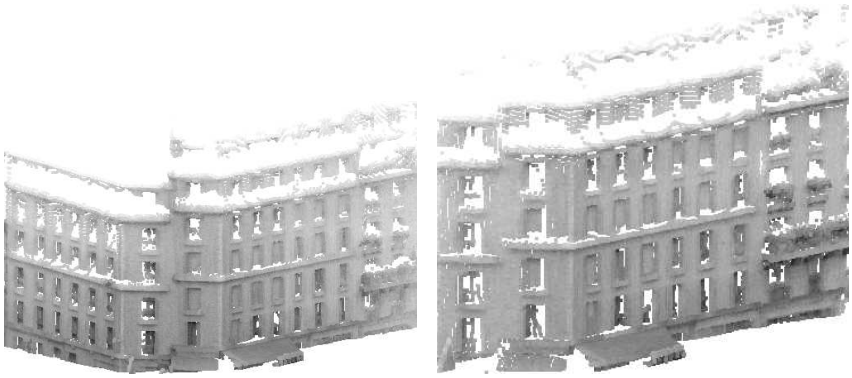

Figure 5: MMS dataset colored using ambient occlusion: two acquisitions of the same area, but with a temporal shift.

5. Experiments

Variants of ICP can be analysed and compared through several criteria: speed, overall accuracy, stability, tolerance to noise or outliers, and maximal initial misalignment. Since we deal with real lidar datasets, we will not tackle the noise/outlier tolerance issue. The problem of initialization will also be put aside since this is out of the scope of the paper. Finally, ICP variant effectiveness

will be assessed with speed and geometrical accuracy performances, considering the stability issue embedded in the discussions of the *matching* step.
Firstly, the comparison protocol will be detailed. Then, it will be applied at each proposed variant of the ICP algorithm, in order to evaluate each of them, and find the best proposition. Therefore, fifteen different solutions have been tested on three datasets. All of them are presented and commented, but variants with the worst results may not be depicted.

5.1. Comparison method

Point cloud registrations can be compared by straightforwardly computing, for each *mobile* point cloud, the mean of the distances of the closest points in the *reference* point cloud. Nevertheless, non-overlapping areas may exist: this value is thus not relevant for that purpose.
To address this issue, the n-resolution $\mathcal{R}_n$ of a point cloud is defined by the mean distance of the n-closest points in the same dataset. In our experiments, the value $n = 5$ is selected, even if the selection of the optimal neighbors may be a better solution. Then, a distance threshold $t = 10 \times \mathcal{R}_n$ has been introduced, and the mean of the distances smaller than t (noted $\bar{t}$) is computed. Finally, the performance of each variant is evaluated through a graph of the final $\bar{t}$ with respect to the convergence speed, computed on a Intel Core2 2.83 GHz CPU with 4 GB of RAM. These results are compared with a *default* configuration, considered at each stage of the registration process. Such a configuration is (see Section 3.1):

- Selecting: all 3D points;
- Matching: closest point;
- Weighting: constant weight w_C;
- Rejecting: none, all corresponding pairs;
- Minimizing: point-to-point distance, without normal computation.

5.2. Selecting

Five variations, as discussed in Section 3.2, have been proposed. The point cloud is first randomly sampled (*random*) and 10% of the points are conserved. Then, only the 3D points with high entropy values (E_f^*) are selected. Two empirical thresholds are tested: $E_f^* > 0.6$, and $E_f^* > 0.7$. Finally, points have been selected according to their dimensionality label, resulting in three cases: $l^* = 1$, $l^* = 2$, and $l^* = 3$. Results are presented in Figure 6.

The first conclusion is that faster registrations can be achieved with proposed selection variants. The accuracy is only increased with $l^* = 2$, which allows to focus on planar surfaces. Improvements are noticed for the three datasets. This is due to the fact that such areas are the most stable with respect to point density and point of view variations.

Speed is significantly improved with all other selection methods, since, indeed, a smaller number of points is introduced in the ICP procedure. While the random subsampling of the point clouds often achieves the worst results, and should be discarded (except for the TLS dataset, where the point density is still very important after reduction). Besides, the entropy-based selection improves the convergence time by a factor of 5 to 7, depending on the value of the threshold. However, the accuracy is slightly lower than the *default* configuration, especially for the ALS dataset. Finally, for such case, the $l^* = 1$ and $l^* = 3$ selections steadily improve the convergence times but not the geometrical accuracy. Such labels correspond in practice, for the airborne case, to building roof top and gutter lines, respectively. A fewer number of points are concerned in the data, resulting in saving computing times. However, as such labeling may vary a lot with changing point densities, it is not so stable and not optimal registration quality is achieved. These results show that the E_f^* feature should be introduced for registration issues where a trade-off between accuracy and computing time has to be found. For highly sampled objects (TLS and MMS datasets), E_f^* is all the more relevant as it allows to tune how confident on the local analysis we are. It is directly related to how well a surface is described with the available point density. Thus, when the point distributions is homogeneous, such as for

the ALS dataset, this solution is less efficient.

5.3. Weighting

Six different weighting functions have been proposed and compared to the *default* configuration : the omnivariance-based weight w_O, the normal compatibility w_N, the eigenvalues-based weight w_λ, the geometrical feature-based weight w_a, and the optimal radius-based weight w_r. Results are presented in Figure 7. The *default* weighting provides the best results in terms of speed for all datasets. Furthermore, slightly similar results to the *default* configuration are achieved in terms of accuracy (but with slower convergence) for the three weights directly related to the shape of the local neighborhood: w_O, w_λ, and w_r. The optimal neighborhood size retrieval thus offers a reliable alternative for the weighting step.

5.4. Rejecting

Finally, for the rejection step, eleven configurations (noted as follows : $2.5\sigma_d$, d_2^{50}, d_2^{70}, d_O^{50}, d_O^{70}, d_{dim}^{50}, d_{dim}^{70}, d_r^{50}, d_r^{70}, d_a^{50}, d_a^{70}) have been proposed, tested on each dataset and compared to the *default* case. Those configurations can be classified into two categories:

1. Distance threshold: Such threshold $2.5\sigma_d$ has to be inferior to 2.5 times the standard deviation of all pair distances.
2. Rank filter: Ten configurations, noted d_α^β, are tested, where α is the distance type and β is the percentage of best matches that are conserved.
    - Five distances are used (see Section 3.3): d_2, d_O, d_{dim}, d_r, and d_a.
    - Two percentages are tested: keeping only the 50% and the 70% of the best matches. These values have been empirically selected among the best 50% matches. They provided the best convergence speed and accuracy results.

Results are depicted in Figure 8. We can first conclude that for each dataset, several new variants improve both the accuracy and the convergence speed of

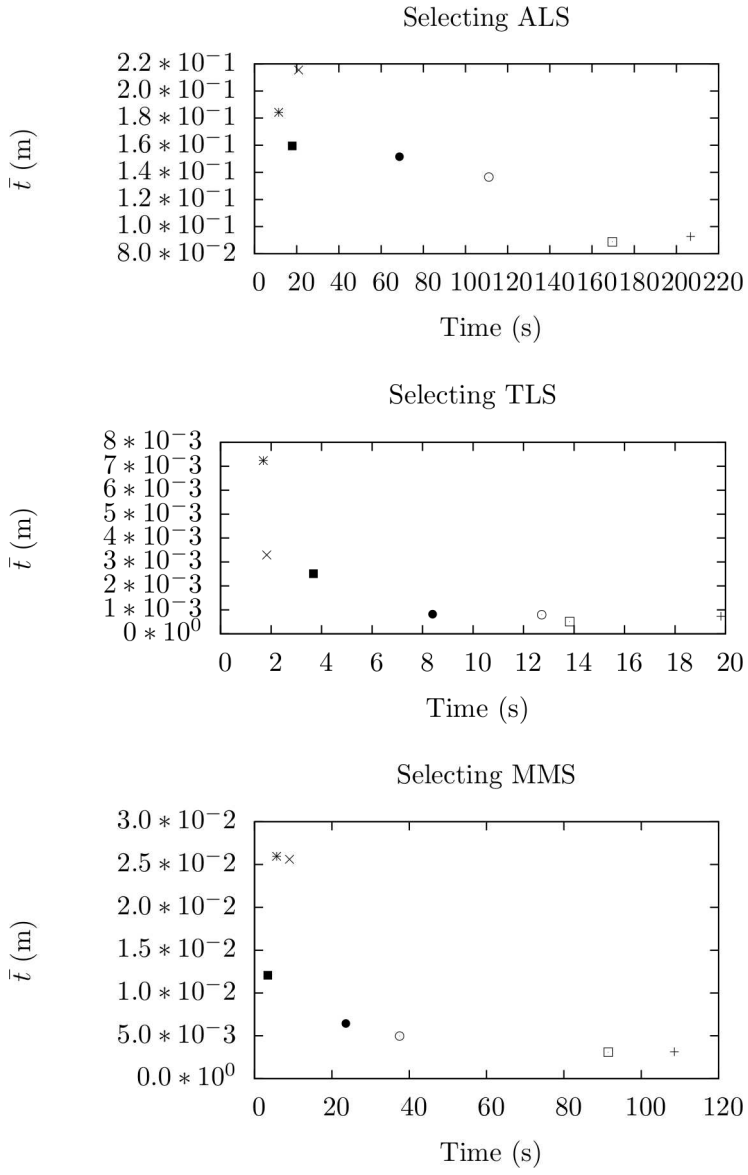

Figure 6: Results of the Selection step.

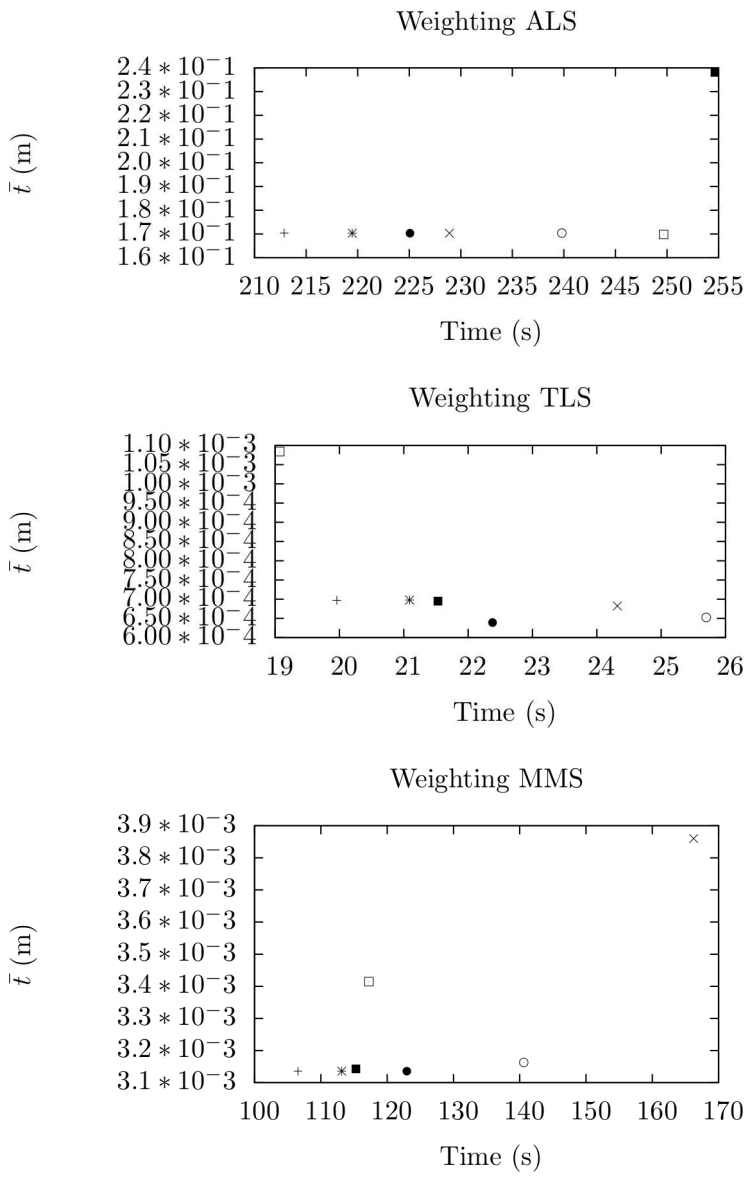

Figure 7: Weighting step results.

the registration. This is particularly true for the TLS and MMS datasets where almost all proposed configurations perform better. For the ALS case, the *default* case remains suitable in terms of speed but provides the worst results in terms of accuracy.

The *distance-threshold* variant can also be discarded since it corresponds to one of the less efficient proposal for the three datasets. Conversely, the omnivariance-based and the geometrical feature-based methods (d_O and d_a, respectively) give the best results for the three datasets with 50% of rejection. The convergence time is improved by a factor of 1.1 to 1.4 when the accuracy is increased up to a factor of 7 for the TLS dataset. Not as good results, especially in terms of speed, are achieved with a greater percentage of rejection. Finally, the Euclidian distance d_2 performs well for the three datasets but only both for speed and accuracy concerns for ALS and TLS datasets.

5.5. Proposal of an optimal variant

As detailed before, the selecting step can be improved by focusing on high entropy points. Besides, the weighting step has no influence on the performance of ICP, and rejecting points using neighborhood-shape criteria (optimal radius or local omnivariance) provides satisfactory results, as illustrated in Figures 9, 10 and 11. This is particularly visible in Figure 11, where no change exists between both surveys. Figures 9 and 10 enhance the relevance of accurate registration for change or mobile object detection since slight shifts can be noticed (cars, vegetation or crane in ALS). Good results are also obtained even when a low overlap exists between both acquisitions (TLS dataset). Finally, the optimal variant is therefore:

- Selecting only points with $E_f^* > 0.7$: It improves the convergence speed by a factor of two while maintaining an accuracy by one tenth of the point cloud resolution. Focus is made on 3D points with a clear local prominent behaviour, *i.e.* in urban areas, building facades for TLS and MMS cases, and ground and building roofs for ALS datasets.

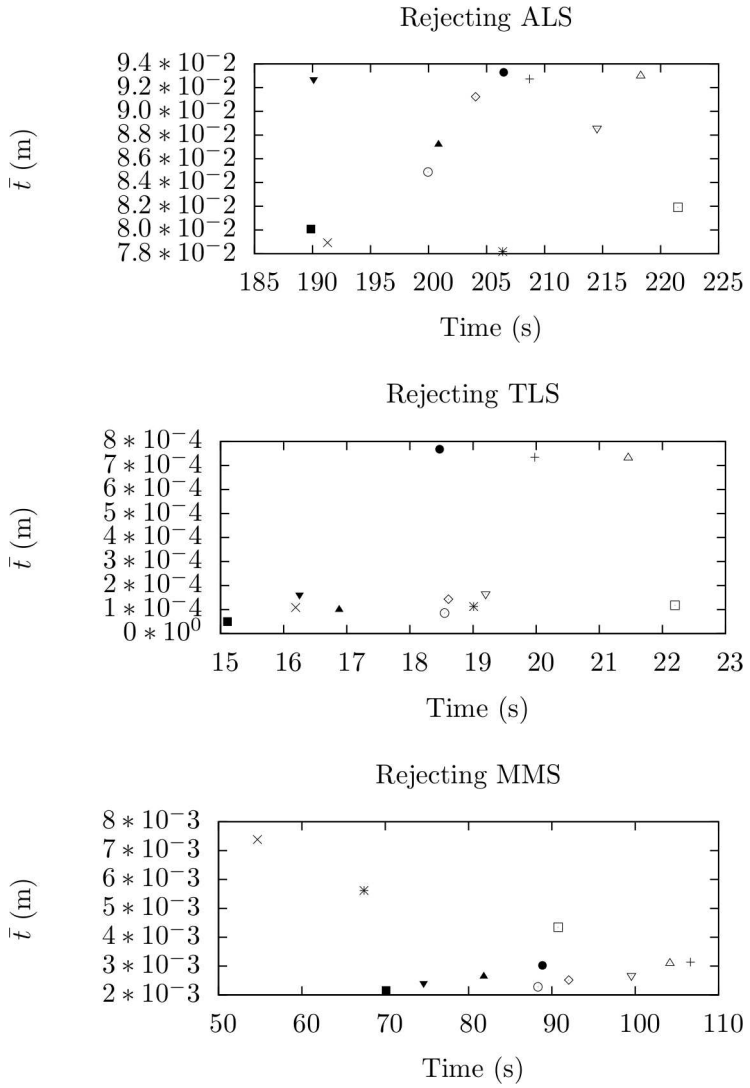

Figure 8: Rejecting step results.

- Weighting: A constant weight is sufficient. The same accuracy can be achieved with other configurations but with higher convergence speed.
- Rejecting: Keeping only the 50% best matches using d_O appears to be the best trade-off between high accuracy and fast convergence speed.

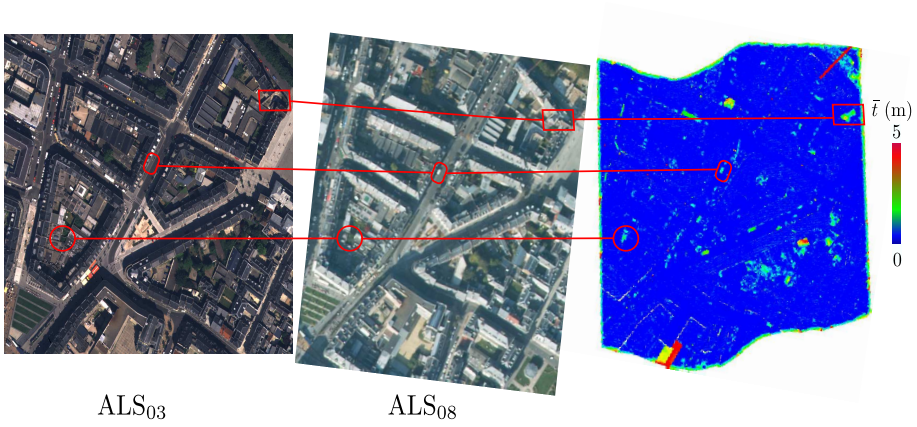

Figure 9: Registration accuracy for the ALS dataset. Left and center: orthoimages temporally coherent with each dataset. Right: Accuracy map. Fine alignment is achieved. Shift between both datasets now correspond to real changes, *e.g.*, new buildings (top area in Figure 9), moving objects like cars (middle area) or vegetation growth (above area).

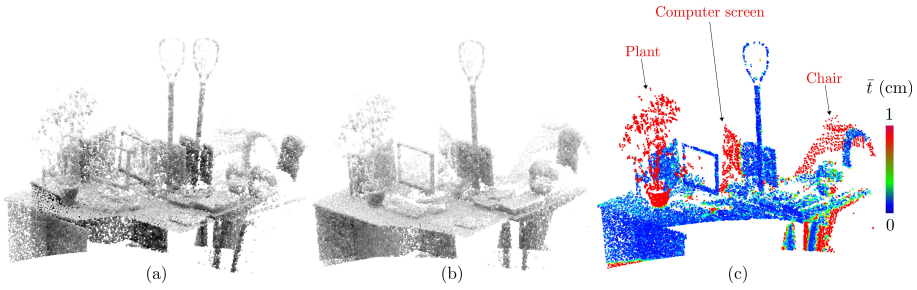

Figure 10: Illustration of the proposed ICP optimal variant for the TLS dataset. (a) Before registration. (b) After registration. (c) Accuracy map. Objects visible in a single scan are clearly enhanced.

The best improvements are retrieved for TLS and MMS datasets i.e. The main limitation of the proposed approach is the failure of improvement of the ALS dataset. This comes from the fact that with fiber scan patterns, the optimal local supports are difficult (1) to retrieve and (2) to be matched with more

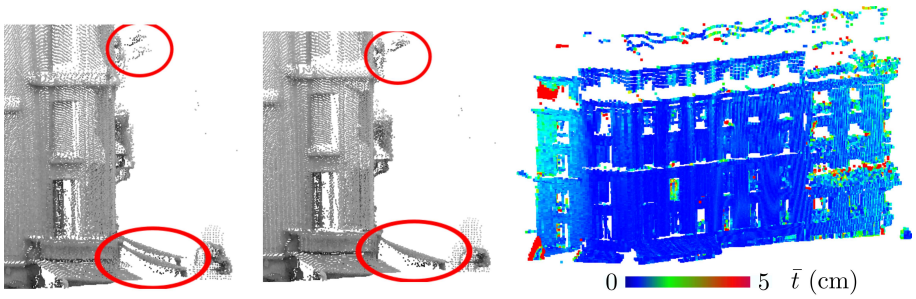

(a) (b) (c)

Figure 11: Optimal configuration alignment for the MMS dataset. (a) Before registration. (b) After registration. (c) Accuracy map. The only discrepancies correspond to areas visible in a single point cloud.

regular sampling of the Earth surface.

6. Conclusion

In this paper, we have demonstrated how the standard and well-known Iterative Closest Point algorithm can be improved by using geometrical features which optimally describe the local shape around of each 3D lidar point. Our method, which both takes into account the neighborhood shape and how confident in the estimate of this shape we are, allowed to improve two of the five steps of the method, namely the selection and rejection issues. Since the computation of the features of interest only requires the knowledge of the position of the 3D points, the method has been tested on datasets acquired from various sensors (airborne, terrestrial static, mobile mapping system). Ten attributes, extracted from a multi-scale local Principal Component Analysis, have been computed. More than twenty variants of the standard ICP procedure have been investigated and analysed in terms of registration accuracy and convergence speed. Even if the three datasets are dissimilar (especially airborne point clouds compared to terrestrial static or mobile ones), general common conclusions can be drawn. First, it is possible to propose an optimal variant, suitable for the three kinds of lidar data, with two salient features (the entropy and the omnivariance). Secondly, very close results are noticed for TLS and MMS datasets since surfaces are

highly and similarly sampled. For the ALS dataset, even if the point densities and the laser scanning patterns were very different, relevant eigenvalue-based solutions have been found. In particular, we have noted that very particular behaviours corresponding to building tops and edges can be interesting as key areas for fast registration.

Consequently, two improvements of our approach are conceivable, so as to provide more efficient features for registration. On the one hand, it appears necessary to fully exploit the multi-scale geometrical analysis. Instead of working only at the most prominent level, the integration of several scales of interest would allow to provide a more specific feature. On the other hand, for datasets acquired with two very different points of view, the local neighborhood (linear, planar, volumetric) shape may not be helpful since it may appear noisy. Conversely, 3D points with no particular prominent dimension seem more stable with varying survey conditions.

Allen, B., Curless, B., Popovíc, Z., 2003. The space of human body shapes: reconstruction and parameterization from range scans. ACM Transactions on Graphics 22 (3), 587–594.

Armenakis, C., Gao, Y., Sohn, G., 2012. Semi-automatic co-registration of photogrammetric and lidar data using buildings. ISPRS Annals of the Photogrammetry, Remote Sensing and Spatial Information Sciences I-3, 13–18.

Bae, K., Lichti, D., 2008. A method for automated registration of unorganised point clouds. ISPRS Journal of Photogrammetry and Remote Sensing 63 (1), 36–54.

Bae, K.-H., 2010. Automated registration of three dimensional unorganised point clouds from terrestrial laser scanners. Ph.D. thesis, Curtin University of Technology, Perth, Australia.

Barnea, S., Filin, S., 2008. Keypoint based autonomous registration of terrestrial laser point-clouds. ISPRS Journal of Photogrammetry and Remote Sensing 63 (1), 19–35.

Bergevin, R., Soucy, M., Gagnon, H., Laurendeau, D., 1996. Towards a general multi-view registration technique. IEEE Transactions on Pattern Analysis and Machine Intelligence 18 (5), 540–547.

Besl, P., McKay, N., 1992. A method for registration of 3-D shapes. IEEE Transactions on Pattern Analysis and Machine Intelligence 14 (2), 239–256.

Bosché, F., 2012. Plane-based registration of construction laser scans with 3d/4d building models. Advanced Engineering Informatics 26 (1), 90–102.

Breitenreicher, D., Schnörr, C., 2011. Model-based multiple rigid object detection and registration in unstructured range data. International Journal of Computer Vision 92 (1), 32–52.

Brodu, N., Lague, D., 2012. 3D terrestrial lidar data classification of complex natural scenes using a multi-scale dimensionality criterion: applications in geomorphology. ISPRS Journal of Photogrammetry and Remote Sensing 68 (2), 121–134.

Chen, C.-S., Hung, Y.-P., Cheng, J.-B., 1999. Ransac-based darces: a new approach to fast automatic registration of partially overlapping range images. IEEE Transactions on Pattern Analysis and Machine Intelligence 21 (11), 1229–1234.

Chen, Y., Medioni, G., 1992. Object modelling by registration of multiple range images. Image Vision Computing 10 (3), 145–155.

Chui, H., Rangarajan, A., Zhang, J., Leonard, C. M., 2004. Unsupervised learning of an atlas from unlabeled point-sets. IEEE Transactions on Pattern Analysis and Machine Intelligence 26 (2), 160–172.

Craciun, D., Paparoditis, N., Schmitt, F., 2010. Multi-view scans alignment for 3d spherical mosaicing in large-scale unstructured environments. Computer Vision and Image Understanding 114 (11), 1248–1263.

Demantké, J., Mallet, C., David, N., Vallet, B., 2011. Dimensionality based scale selection in 3D lidar point cloud. The International Archives of the Photogrammetry, Remote Sensing and Spatial Information Sciences 38 (Part 5/W12), (on CD-ROM).

Digne, J., Morel, J.-M., 2012. A numerical analysis of differential operators on raw point clouds. Tech. Rep. CMLA-2011-03, CMLA, ENS Cachan, France.

Digne, J., Morel, J.-M., Souzani, C.-M., Lartigue, C., 2011. Scale space meshing of raw data point sets. Computer Graphics Forum 30 (6), 1630–1642.

Dold, C., Brenner, C., 2006. Registration of terrestrial laser scanning data using planar patches and image data. International Archives of Photogrammetry, Remote Sensing and Spatial Information Sciences 36 (Part 5), 78–83.

Douillard, B., Quadros, A., Morton, P., Underwood, J., Deuge, M. D., Hugosson, S., Hallström, M., Bailey, T., 2012. Scan segments matching for pairwise 3d alignment. In: International Conference on Robotics and Automation. IEEE, Saint-Paul, MI, USA, 14-18 May 2012, pp. 3033–3040.

Frome, A., Huber, D., Kolluri, R., Bülow, T., Malik, J., 2004. Recognizing objects in range data using regional point descriptors. In: IEEE European Conference on Computer Vision. IEEE, Prague, Czech Republic, 11-14 May 2004.

Gelfand, N., Ikemoto, L., Rusinkiewicz, S., Levoy, M., 2003. Geometrically stable sampling for the icp algorithm. In: International Conference on 3D Digital Imaging and Modeling. IEEE, Banff, Alberta, Canada, 6-10 October 2003, pp. 260–267.

Godin, G., Rioux, M., Baribeau, R., 1994. Three-dimensional registration using range and intensity information. In: Proc. of SPIE: Videometrics III, SPIE, 6 October 1994. Vol. 2350. pp. 279–290.

Grant, D., Bethel, J., Crawford, M., 2012. Point-to-plane registration of terrestrial laser scans. ISPRS Journal of Photogrammetry and Remote Sensing 72 (2), 16–26.

Gressin, A., Mallet, C., David, N., 2012. Improving 3d lidar point cloud registration using optimal neighborhood knowledge. ISPRS Annals of Photogrammetry, Remote Sensing and Spatial Information Sciences I-3, 111–116.

Gross, H., Thoennessen, U., 2006. Extraction of lines from laser point clouds. The International Archives of Photogrammetry, Remote Sensing and Spatial Information Sciences 36 (Part 3), 86–91.

Gruen, A., Akca, D., 2005. Least squares 3d surface and curve matching. ISPRS Journal of Photogrammetry and Remote Sensing 59 (3), 151–174.

Ho, J., Peter, A., Rangarajan, A., Yang, M.-H., 2009. An algebraic approach to affine registration of point sets. In: IEEE International Conference on Computer Vision. IEEE, Kyoto, Japan, 27 September-4 October 2009.

Huber, D., Hebert, M., 2003a. 3d modeling using a statistical sensor model and stochastic search. In: IEEE Conference on Computer Vision and Pattern Recognition. IEEE, Madison, WI, USA, 16-22 June 2003, pp. 858–865.

Huber, D., Hebert, M., 2003b. Fully automatic registration of multiple 3d data sets. Image and Vision Computing 21 (7), 637–650.

Jutzi, B., Gross, H., 2009. Nearest neighbour classification on laser point clouds to gain object structures from buildings. The International Archives of the Photogrammetry, Remote Sensing and Spatial Information Sciences 38 (Part 5), on CD–ROM.

Li, H., Hartley, R., 2007. The 3d-3d registration problem revisited. In: IEEE International Conference on Computer Vision. IEEE, Rio de Janeiro, Brazil, 14-20 October 2007.

Lichti, D., Skaloud, J., 2010. Airborne and Terrestrial laser scanning. CRC Press, Boca Raton, FL, USA, Ch. Registration and Calibration.

Lohr, U., Eibert, M., 1995. The toposys laser scanner-system. In: The Photogrammetric Week. Stuttgart, Germany, pp. 263–267.

Lu, F., Milos, E., 1997. Robot pose estimation in unknown environments by matching 2d range scans. Journal of Intelligent Robotics Systems 18 (3), 249–275.

Makadia, A., Patterson, A., Daniilidis, K., 2006. Fully automatic registration of 3d point clouds. In: IEEE Conference on Computer Vision and Pattern Recognition. IEEE, New-York, NY, USA, 17-22 June 2006, pp. 1297–1304.

Masuda, T., Sakaue, K., Yokoya, N., 1996. Registration and integration of multiple range images for 3-d model construction. In: Proc. of the International Conference on Pattern Recognition, IAPR, 25-30 August 1996. Vienna, Austria, pp. 879–883.

Mitra, N., Gelfand, N., Pottmann, H., Guibas, L., 2004. Registration of point cloud data from a geometric optimization perspective. In: Eurographics Symposium on Geometry Processing. Vol. 12. ACM, Nice, France, 8-10 July 2004.

Myronenko, A., Song, X., 2010. Point set registration: Coherent point drift. IEEE Transactions on Pattern Analysis and Machine Intelligence 32 (12), 2262–2275.

Novatnack, J., Nishino, K., 2007. Scale-dependent 3d geometric features. In: IEEE International Conference on Computer Vision. IEEE, Rio de Janeiro, Brazil, 14-20 October 2007.

Papazov, C., Burschka, D., 2011. Deformable 3d shape registration based on local similarity transforms. Computer Graphics Forum 30 (5), 1492–1503.

Pauly, M., Keiser, R., Gross, M., 2003. Multi-scale feature extraction on point-sampled surfaces 22 (3), 281–289.

Pulli, K., 1999. Multiview registration for large data sets. In: Proc. of the International Conference on 3D Digital Imaging and Modeling (3DIM), IEEE, 4-8 October 1999. Ottawa, Canada, pp. 160–168.

Rabbani, T., Dijkman, S., van den Heuvel, F., Vosselman, G., 2007. An integrated approach for modelling and global registration of point clouds. ISPRS Journal of Photogrammetry and Remote Sensing 61 (6), 355–370.

Ripperda, N., Brenner, C., 2005. Marker-free registration of terrestrial laser scans using the normal distribution transform. International Archives of Photogrammetry, Remote Sensing and Spatial Information Sciences 36 (Part 5-W17), (on CD-ROM), 86–91.

Rodrigues, M., Fisher, R., Liu, Y., 2002. Special issue on registration and fusion of range images. Computer Vision and Image Understanding 87 (1-2), 1–7.

Rusinkiewicz, S., Levoy, M., 2001. Efficient variants of the ICP algorithm. In: Proc. of the International Conference on 3D Digital Imaging and Modeling, IEEE, 28 May-1 June 2001. Québec, Canada, pp. 145–152.

Salvi, J., Matabosch, C., Fofi, D., Forest, J., 2007. A review of recent range image registratioon methods with accuracy evaluation. Image Vision Computing 25 (5), 578–596.

Segal, A., Haehnel, D., Thrun, S., 2009. Generalized-icp. In: Proceedings of Robotics: Science and Systems. Seattle, USA.

Sharp, G., Lee, S., D.K., W., 2002. ICP registration using invariant features. IEEE Transactions on Pattern Analysis and Machine Intelligence 24 (1), 90–102.

Silva, L., Bellon, O., Boyer, K., 2005. Precision range image registration using a robust surface interpenetration measure and enhanced genetic algorithms. IEEE Transactions on Pattern Analysis and Machine Intelligence 27 (5), 762–776.

Stamos, I., Leordeanu, M., 2003. Automated feature-based range registration of urban scenes of large scale. In: IEEE Conference on Computer Vision and Pattern Recognition. IEEE, Madison, WI, USA, 16-22 June 2003.

Stein, F., Medioni, G., 1992. Structural indexing: Efficient 3-d object recognition. IEEE Transactions on Pattern Analysis and Machine Intelligence 14 (2), 125–145.

Szeliski, R., Lavallée, S., 1996. Matching 3-d anatomical surfaces with non-rigid deformations using octree-splines. International Journal of Computer Vision 18, 171–186.

Theiler, P., Schindler, K., 2012. Automatic registration of terrestrial laser scanner point clouds using natural planar surfaces. The International Annals of Photogrammetry, Remote Sensing and Spatial Information Sciences 39 (Part 3), 86–91.

Thirion, J. P., 1996. Feature points based on geometric invariants for 3d image registration. International Journal of Computer Vision 18 (2), 121–137.

Tsin, Y., Kanade, T., 2004. A correlation-based approach to robust point set registration. In: IEEE European Conference on Computer Vision. IEEE, Prague, Czech Republic, 11-14 May 2004, pp. 558–569.

Turk, G., Levoy, M., 1994. Zippered polygon meshes from range images. In: Proc. SIGGRAPH, ACM, 24-29 July 1994. Orlando, FL, USA, pp. 311–318.

Unnikrishnan, R., Hebert, M., 2008. Multi-scale interest regions from unorganized point clouds. In: Workshop on Search in 3D (S3D), IEEE Conference on Computer Vision and Pattern Recognition. IEEE, Anchorage, AK, USA, 24-26 June 2008.

Unnikrishnan, R., Lalonde, J.-F., Vandapel, N., Hebert, M., October 2010. Scale selection for geometric fitting in noisy point clouds. International Journal of Computational Geometry & Applications 20 (5), 543–575.

Weinmann, M., Weinmann, M., Hinz, S., Jutzi, B., 2011. Fast and automatic image-based registration of tls data. ISPRS Journal of Photogrammetry and Remote Sensing 66 (6), S62–S70.